Molecular Therapy
Methods & Clinical Development
Original Article

Dual-AAV vector-mediated expression of *MYO7A* improves vestibular function in a mouse model of Usher syndrome 1B

Samantha C. Lau,[1] Mhamed Grati,[1] Kevin Isgrig,[1] Moaz Sinan,[1] Kaitlyn R. Calabro,[2] Jianliang Zhu,[1] Yasuko Ishibashi,[1,4] Zeynep Ozgur,[1] Talah Wafa,[3] Inna A. Belyantseva,[4] Tracy Fitzgerald,[3] Thomas B. Friedman,[4] Sanford L. Boye,[5] Shannon E. Boye,[2] and Wade W. Chien[1,6]

[1]Inner Ear Gene Therapy Program, National Institute on Deafness and Other Communication Disorders, National Institutes of Health, Bethesda, MD 20892, USA; [2]Division of Cellular and Molecular Therapy, Department of Pediatrics, University of Florida, Gainesville, FL, USA; [3]Mouse Auditory Testing Core Facility, National Institute on Deafness and Other Communication Disorders, National Institutes of Health, Bethesda, MD 20892, USA; [4]Laboratory of Molecular Genetics, National Institute on Deafness and Other Communication Disorders, National Institutes of Health, Bethesda, MD 20892, USA; [5]Powell Gene Therapy Center, Department of Pediatrics, University of Florida, Gainesville, FL, USA; [6]Department of Otolaryngology – Head & Neck Surgery, Johns Hopkins School of Medicine, Baltimore, MD, USA

Usher syndrome is the most common cause of deafness-blindness in the world. Usher syndrome type 1B (USH1B) is associated with mutations in *MYO7A*. Patients with USH1B experience deafness, blindness, and vestibular dysfunction. In this study, we applied adeno-associated virus (AAV)-mediated gene therapy to the shaker-1 (*Myo7a*$^{4626SB/4626SB}$) mouse, a model of USH1B. The shaker-1 mouse has a nonsense mutation in *Myo7a*, is profoundly deaf throughout life, and has significant vestibular dysfunction. Because of the ~6.7-kb size of the *MYO7A* cDNA, a dual-AAV approach was used for gene delivery, which involves splitting human *MYO7A* cDNA into 5′ and 3′ halves and cloning them into two separate AAV8(Y733F) vectors. When *MYO7A* cDNA was delivered to shaker-1 inner ears using the dual-AAV approach, cochlear hair cell survival was improved. However, stereocilium organization and auditory function were not improved. In contrast, in the vestibular system, dual-AAV-mediated *MYO7A* delivery significantly rescued hair cell stereocilium morphology and improved vestibular function, as reflected in a reduction of circling behavior and improved vestibular sensory-evoked potential (VsEP) thresholds. Our data indicate that dual-AAV-mediated MYO7A expression improves vestibular function in shaker-1 mice and supports further development of this approach for the treatment of disabling dizziness from vestibular dysfunction in USH1B patients.

INTRODUCTION

Usher syndrome (USH) is the most common cause of inherited deafness-blindness.[1] Its prevalence ranges from 3.2–6.5 per 100,000 people depending on the population.[2,3] USH is inherited in an autosomal-recessive pattern and is classified into three major clinical subtypes (types 1–3), with type 1 patients having the most clinically severe phenotype.[4] USH type 1B (USH1B) is the most common form of USH type 1[5] and is associated with variants in *MYO7A* (MIM: 276900).[4,6] Patients with USH1B are born with profound hearing loss and vestibular dysfunction and develop progressive loss of vision because of retinitis pigmentosa during the first decade of life.[7] The *MYO7A* gene encodes the unconventional MYO7A,[6,8] and it is expressed in mechanosensory hair cells in the inner ear, photoreceptors, and retinal pigment epithelium cells.[8,9] Recent studies have shown that adeno-associated virus (AAV)-mediated gene replacement therapy can be used to improve the auditory and vestibular functions in several mouse models of USH.[10] However, the challenge of applying AAV-mediated gene replacement therapy to mouse models of USH1B is the fact that the cDNA of *MYO7A* is ~6.7 kb in length, which exceeds the ~4.7-kb carrying capacity of AAV.[11,12]

One way of overcoming this challenge is to use a dual-AAV vector-based approach, which divides a large cDNA into two halves and utilizes two separate AAV expression cassettes to deliver these cDNA fragments.[13,14] The first vector contains the promoter and 5′ half of the cDNA, whereas the second vector contains the 3′ half of the cDNA along with the polyadenylation signal. When both capsids co-infect the same cell, these 5′ and 3′ cDNA halves recombine to form the full-length coding sequence and generate full-length protein. There are two major dual vector strategies that promote recombination and generation of full-length protein: overlapping and hybrid.[13,14] "Overlap" dual vectors contain cDNA fragments with complementary genetic sequences that drive homologous recombination. "Hybrid" dual vectors rely on a recombinogenic sequence from the human placental *ALPL* gene (which encodes alkaline phosphatase [AP]) to promote recombination[15] and splice donor and acceptor

Received 14 March 2023; accepted 16 August 2023;
https://doi.org/10.1016/j.omtm.2023.08.012.

Correspondence: Wade W. Chien, Inner Ear Gene Therapy Program, National Institute on Deafness and Other Communication Disorders, National Institutes of Health, Bethesda, MD 20892, USA.
E-mail: wade.chien@nih.gov

sites for excision of the intervening sequence from the resulting transcript. In a study by Dyka et al.,[13] these dual-AAV strategies were compared for their ability to drive full-length MYO7A expression *in vitro* and *in vivo*. They found that the hybrid strategy resulted in the highest level of full-length MYO7A expression. They also showed that subretinal injection of the hybrid dual-AAV vectors carrying human *MYO7A* cDNA was capable of producing human MYO7A expression in the C57BL/6J mouse retina.[13] Similarly, in another study by Trapani et al.,[14] these different dual-AAV strategies were tested, and it was found that the hybrid strategy was highly effective at delivering human *MYO7A* cDNA and promoting expression of full-length MYO7A *in vitro*. In addition, sub-retinal injection of the hybrid dual-AAV vectors carrying human *MYO7A* cDNA into a *Myo7a* mutant mouse (shaker-1, $Myo7a^{4626SB/4626SB}$) resulted in expression of full-length human MYO7A and improvement of melanosome and rhodopsin localization in the mouse retina.[14]

In this study, we asked whether hybrid dual-AAV vectors could mediate sufficient levels of full-length MYO7A expression in the inner ear of the shaker-1 mouse model for USH1B. The deaf shaker-1 mouse has a nonsense mutation in *Myo7a* and has significant vestibular dysfunction throughout life.[6,16] We injected hybrid dual-AAV vectors carrying the human *MYO7A* cDNA into neonatal shaker-1 mice through the posterior semicircular canal (PSC) and evaluated whether gene replacement therapy could improve auditory and vestibular function in these mutant mice.

RESULTS

Dual-AAV8(Y733F) vectors restore MYO7A expression in cochlear hair cells

The shaker-1 ($Myo7a^{4626SB/4626SB}$) mutant mouse has a nonsense mutation in *Myo7a* and is considered a null mutant.[17,18] To restore MYO7A expression in shaker-1 mice, we utilized the hybrid dual-AAV vectors packaged in AAV8(Y733F).[13] The 5′ vector contains the ubiquitous CMV/chicken β-actin (smCBA) promoter, the 5′ portion of human *MYO7A* cDNA (2,904 bp), a splice donor, and a recombinogenic sequence derived from a coding sequence for AP (287 bp, labeled "AP"). The 3′ vector contains a complementary AP coding sequence, a splice acceptor, the 3′ portion of human *MYO7A* cDNA (3,627 bp), a hemagglutinin (HA) tag, and a polyadenylation signal (Figure S1A). We call this set of dual-AAV vectors "dual-AAV8(Y733F)-*MYO7A*." The human *MYO7A* cDNA was used in this study instead of the mouse *Myo7a* cDNA because it is the human *MYO7A* cDNA that will be used for clinical translation in USH1B patients in the future. In addition, the human *MYO7A* cDNA has been successfully delivered into the mouse retina using the dual-AAV approach.[13,14] Subretinal injection of these dual-AAV8(Y733F)-*MYO7A* vectors in $Myo7a^{-/-}$ mice results in full-length MYO7A protein expression.[19] Infection of these vectors in COS-7 cells resulted in the detection of MYO7A expression with anti-MYO7A or anti-HA-tag antibodies directed against the N-terminal, middle, and C-terminal (HA) portions of the protein sequence (Figure S1B). In addition, the antibody targeting the middle portion of MYO7A, which was used for the rest of the study, only detected MYO7A expression when the 5′ and 3′ vectors were used to infect COS-7 cells (Figure S1C). These results confirm that dual-AAV8(Y733F)-*MYO7A* vectors can produce full-length MYO7A expression in infected cells.

Using the PSC approach, we microinjected dual-AAV8(Y733F)-*MYO7A* (0.5 μL of the 5′ vector and 0.5 μL of the 3′ vector) into the inner ears of live neonatal (post-natal day 0 [P0]–P4) shaker-1 mouse pups. The cochleae of these animals were then dissected at P30–P37 and examined using immunofluorescence and confocal microscopy. In untreated wild-type and heterozygous shaker-1 mice, we found that MYO7A was highly expressed in the inner hair cells (IHCs) and outer hair cells (OHCs) of the cochlea. In contrast, we were unable to detect MYO7A expression in the cochlea of shaker-1 mutant mice (Figure 1A). When dual-AAV8(Y733F)-*MYO7A* vectors were injected into shaker-1 inner ears, MYO7A expression was restored in the transduced IHCs and OHCs (Figure 1A). The IHC transduction rate was 77% ± 12% at the apex, 77% ± 11% at the middle turn, and 47% ± 12% at the base of the cochlea (Figure 1B; n = 6 mice). The OHC transduction rate was 82% ± 16% at the apex, 45% ± 18% at the middle turn, and 22% ± 9.5% at the base of the cochlea (Figure 1C; n = 6 mice). MYO7A expression in the IHCs and OHCs of the injected shaker-1 mice also co-localized with HA expression, indicating that the MYO7A expression seen in the injected shaker-1 mice was a result of the dual-AAV8(Y733F)-*MYO7A* treatment (Figure S2). Our results indicate that dual-AAV8(Y733F)-*MYO7A* treatment restored MYO7A protein expression in the transduced shaker-1 IHCs and OHCs.

Dual-AAV8(Y733F)-*MYO7A* vectors improve IHC and OHC survival in the shaker-1 cochlea

IHCs and OHCs in the shaker-1 mouse undergo significant degeneration (Figure 1A). Therefore, we wanted to examine whether dual-AAV vector treatment could improve IHC and OHC survival in the treated shaker-1 mouse. At ∼P30, the average IHC count for the wild-type mouse was 15 ± 0.47 cells/136 μm at the apex, 17 ± 0.75 cells/136 μm at the middle turn, and 16 ± 0.25 cells/136 μm at the base of the cochlea (Figure 1D; n = 4 mice). The average IHC count for the untreated shaker-1 mouse was 6.9 ± 1.4 cells/136 μm at the apex, 3.3 ± 1.5 cells/136 μm at the middle turn, and 2.4 ± 1.5 cells/136 μm at the base of the cochlea (Figure 1D; n = 5 mice). When dual-AAV8(Y733F)-*MYO7A* vectors were injected into the shaker-1 mouse, we noticed a significantly higher number of surviving IHCs in treated shaker-1 mice compared with untreated homozygous mutants ($p < 0.0001$, two-way ANOVA). For shaker-1 mice that were treated with dual-AAV8(Y733F)-*MYO7A*, the average IHC count was 14 ± 1.2 cells/136 μm at the apex ($p = 0.003$ compared with the untreated mutants), 14 ± 1.9 cells/136 μm at the middle turn ($p < 0.0001$ compared with the untreated mutants), and 7.3 ± 1.8 cells/136 μm at the base of the cochlea ($p = 0.06$ compared with the untreated mutants), respectively (Figure 1D; n = 6 mice, ANOVA with Tukey's multiple-comparisons test). The magnitude of preservation was consistent with the relative levels of transduction

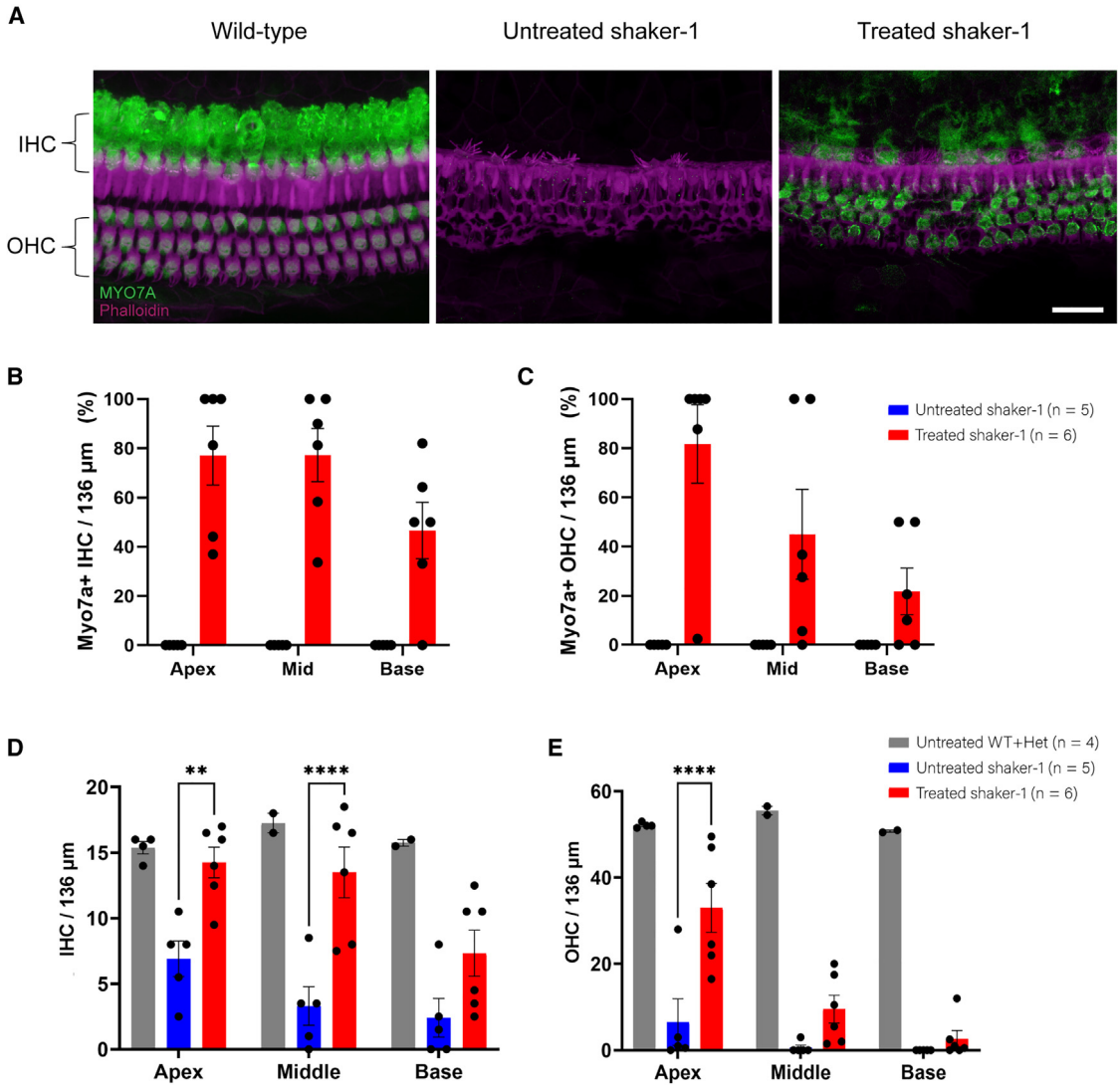

Figure 1. Dual-AAV8(Y733F)-*MYO7A* vectors restore MYO7A expression and prolong the survival of shaker-1 cochlear hair cells

(A) Representative confocal images of inner hair cells (IHCs) and outer hair cells (OHCs) of the cochlear middle turn. In an untreated wild-type mouse, MYO7A expression (green) is found in the IHCs and OHCs. The shaker-1 mouse does not express MYO7A. Shaker-1 mice that were treated with dual-AAV8(Y733F)-*MYO7A* vectors exhibit restoration of MYO7A in transduced IHCs and OHCs. Images were taken at P30–P37. The scale bar represents 20 µm. (B and C) Quantification of IHC (B) and OHC (C) transduction rates in shaker-1 mice that were treated with dual-AAV8(Y733F)-*MYO7A* vectors. (D and E) Quantification of IHC (D) and OHC (E) survival in shaker-1 mice that were treated with dual-AAV8(Y733F)-*MYO7A* vectors. Shaker-1 mice that were treated with dual-AAV8(Y733F)-*MYO7A* vectors showed significant improvement in hair cell survival compared with untreated shaker-1 mice. n = the number of animals used. Error bars represent standard errors. **$p < 0.01$, ****$p < 0.0001$.

in these different regions by our dual vectors (i.e., apex > middle turn > base).

Similar results were observed for OHC survival. The average OHC count in wild-type mice was 52 ± 0.32 cells/136 µm at the apex, 56 ± 1.0 cells/136 µm at the middle turn, and 51 ± 0.25 cells/136 µm at the base of the cochlea (Figure 1E; n = 4 mice). The average OHC count for the untreated shaker-1 mice was 6.5 ± 5.4 cells/136 µm at the apex, 0.60 ± 0.60 cells/136 µm at the middle turn, and 0.0 ± 0.0 cells/136 µm at the base of the cochlea (Figure 1E; n = 5 mice). Injection with dual-AAV8(Y733F)-*MYO7A* vectors resulted in significant preservation of OHCs in the shaker-1 mice ($p < 0.0001$, two-way ANOVA). For shaker-1 mice that were treated with dual-AAV8(Y733F)-*MYO7A*, the average OHC count was 33 ± 5.7 cells/136 µm at the apex ($p < 0.0001$ compared with the untreated mutants), 9.5 ± 3.2 cells/136 µm at the middle turn ($p = 0.2$ compared with the untreated mutants), and 2.7 ± 1.9 cells/136 µm at the base of the cochlea ($p = 0.8$ compared with the untreated mutants), respectively (Figure 1E; n = 6 mice, ANOVA with Tukey's multiple-comparisons test). As seen for IHCs, the magnitude of structural preservation

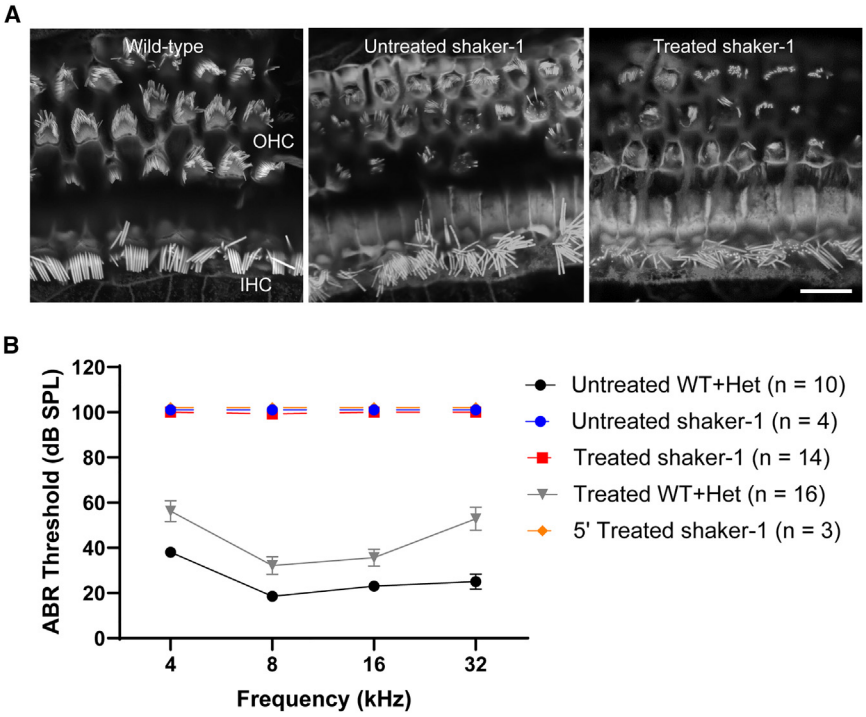

Figure 2. Dual-AAV8(Y733F)-*MYO7A* vectors did not improve stereocilium organization of cochlear hair cells or auditory function in shaker-1 mice

(A) Representative confocal images showing stereocilium organization in IHCs and OHCs. Shaker-1 mice have highly disorganized stereocilium bundles compared to wild-type animals. Dual-AAV8(Y733F)-*MYO7A* vectors did not improve stereocilium organization in shaker-1 cochlear hair cells, as revealed by phalloidin staining to visualize F-actin. The scale bar represents 10 μm. (B) Auditory brain stem response (ABR) thresholds at the four measured frequencies (4, 8, 16, and 32 kHz). An ABR threshold of 100 dB SPL represents no response. ABR testing was done at ∼P30. Dual-AAV8(Y733F)-*MYO7A* vectors did not improve ABR in shaker-1 mice. Error bars represent standard errors.

observed for OHCs was consistent with the relative levels of transduction in these different regions by our dual vectors (i.e., apex > middle turn > base). Our results indicate that dual-AAV8(Y733F)-*MYO7A* treatment improved IHC and OHC survival in shaker-1 mice.

Dual-AAV8(Y733F)-*MYO7A* vectors did not improve cochlear stereocilium organization or auditory function in shaker-1 mice

Stereocilium bundles on the apical surface of hair cells play a critical role in mechanotransduction of auditory information. In wild-type mice, stereocilium bundles are organized in a cohesive staircase-like pattern of stereocilium rows (Figure 2A). In shaker-1 mice, IHCs and OHC stereocilium bundles are highly disorganized from birth, because of the loss of MYO7A that is required for the organization and stabilization of several stereocilium sub-compartmental links (Figure 2A).[20,21] We examined the effect of dual-AAV8(Y733F)-*MYO7A* vectors on the stereocilium bundle organization in the cochlear hair cells of treated shaker-1 mice and observed that stereocilium bundles remained highly disorganized in IHCs and OHCs, similar to those in untreated shaker-1 homozygous mutant mice (Figure 2A).

We further examined auditory function in treated shaker-1 mice using tone-burst auditory brainstem response (ABR) testing at ∼P30 (Figure 2B). In wild-type and heterozygous mice, the average ABR thresholds were 18.5–38 dB from 4–32 kHz (Figure 2B; n = 10 mice). In untreated shaker-1 mutant mice, no measurable ABR waveforms were detected even at the maximal stimulus level of 90 dB (Figure 2B; n = 4 mice). In shaker-1 mutant mice that were treated with dual-AAV8(Y733F)-*MYO7A* vectors, no measurable ABR waveforms were detected, comparable with responses obtained in untreated shaker-1 mutant mice (Figure 2B; n = 14 mice). Some shaker-1 mutant mice were treated with the single AAV8(Y733F) vector carrying the 5′ *MYO7A* cDNA (5′ AAV8(Y733F), 3.3×10^9 GC) as a control, and no measurable ABR waveforms were observed in these animals (Figure 2B; n = 3 mice). Interestingly, in wild-type and heterozygous littermates that were treated with dual-AAV8(Y733F)-*MYO7A* vectors, a ∼10–30 dB ABR threshold elevation was observed compared with untreated wild-type and heterozygous littermates (Figure 2B; n = 16 mice, $p < 0.0001$, ANOVA with Tukey's multiple-comparisons test). A similar ABR threshold elevation was observed in wild-type and heterozygous littermates that were treated with the 5′ AAV8(Y733F) vector alone (n = 4 mice) or AAV8(Y733F)-GFP (7.7×10^9 GC, n = 3 mice) compared with untreated wild-type and heterozygous littermates (Figure S3; $p = 0.0007$ and 0.002, respectively; ANOVA with Tukey's multiple-comparisons test). In contrast, wild-type and heterozygous littermates that were treated with vehicle alone (PBS with 5% glycerol) showed no statistically significant ABR threshold elevation compared with untreated wild-type and heterozygous littermates (Figure S3; n = 5 mice, $p = 0.3$, ANOVA with Tukey's multiple-comparisons test). These results suggest that the ABR threshold elevation observed in wild-type and heterozygous littermates that were treated with dual-AAV8(Y733F)-*MYO7A* vectors is not due to surgical trauma to the inner ear but, rather, the dual-AAV8(Y733F)-*MYO7A* vectors. In summary, our results suggest that dual-AAV8(Y733F)-*MYO7A* vectors were unable to restore cochlear stereocilium organization and auditory function in the shaker-1 homozygous mutant mouse.

Dual-AAV8(Y733F)-*MYO7A* vectors restore MYO7A expression in vestibular hair cells

One of the hallmarks of the shaker-1 mouse phenotype is vestibular dysfunction manifesting as repetitive circling, which is due to the lack of MYO7A expression in vestibular hair cells.[22] We have reported previously that inner ear gene delivery via the PSC approach can effectively transduce hair cells in the cochlea and vestibular

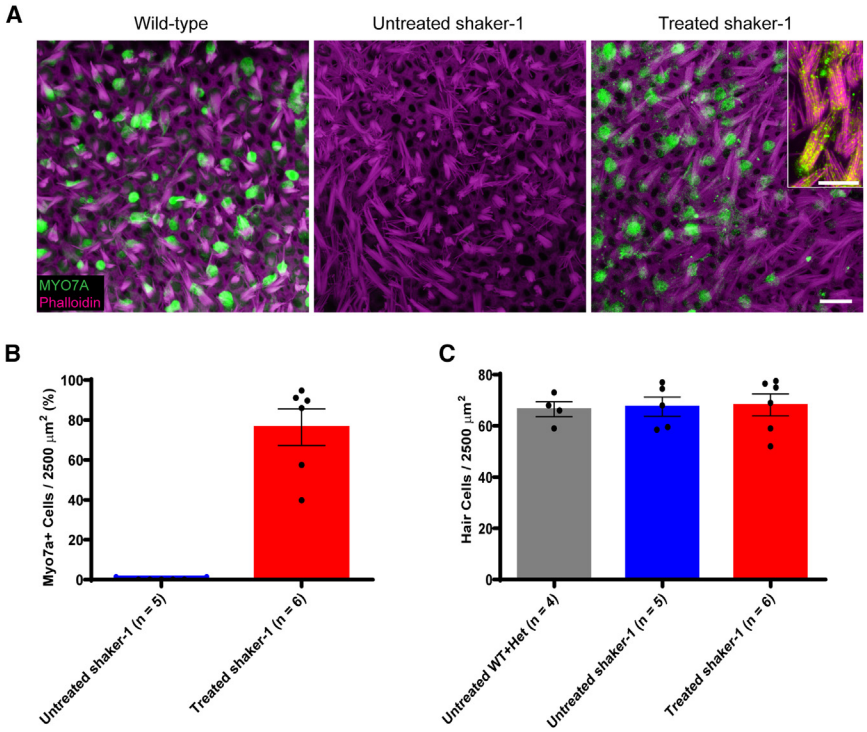

Figure 3. Dual-AV8(Y733F)-*MYO7A* vectors restore MYO7A expression in transduced vestibular hair cells

(A) Representative confocal images of vestibular hair cells from mouse utricles. Images were taken at P30–P37. The shaker-1 mice that were treated with dual-AAV8(Y733F)-*MYO7A* showed robust MYO7A expression (green), whereas the untreated shaker-1 mice showed no MYO7A expression. A higher-magnification view of the treated shaker-1 stereocilia revealed MYO7A expression along the stereocilia bundles (inset). Scale bars represent 10 μm. (B) Quantification of vestibular hair cell transduction rates. (C) Quantification of hair cell survival in mouse utricles. In contrast to the shaker-1 cochlear hair cells, the vestibular hair cells do not undergo degeneration in shaker-1 mice. Error bars represent standard errors.

organs simultaneously.[23,24] Therefore, we examined the transduction efficiency and physiological effects of dual-AAV8(Y733F)-*MYO7A* vectors in the vestibular system of shaker-1 mice. In the wild-type mouse, MYO7A expression is detected in all vestibular hair cells (Figure 3A). In contrast, the homozygous shaker-1 mutant mouse does not express MYO7A in the vestibular organs (Figure 3A). When dual-AAV8(Y733F)-*MYO7A* vectors were delivered into the shaker-1 inner ears, MYO7A expression was restored in the transduced vestibular hair cells (Figure 3A). The vestibular hair cell transduction rate was 77% ± 9.2% in the utricle (Figure 3B; n = 6 mice).

In the shaker-1 cochlea, IHCs and OHCs show signs of severe defects postnatally and undergo rapid degeneration (Figure 1A). Therefore, we wanted to see whether similar hair cell degeneration also occurs in the vestibular system. In wild-type mice, the average vestibular hair cell count was 67 ± 2.9 cells/2,500 μm^2 (Figure 3C; n = 4 mice). Surprisingly, at 1 month of age, the vestibular hair cell count in untreated shaker-1 mice was similar to the wild-type mouse, with the average vestibular hair cell count of 68 ± 3.8 cells/2,500 μm^2 (n = 5 mice, p > 0.9, ANOVA with Tukey's multiple-comparisons test) (Figure 3C). In shaker-1 mice that were treated with dual-AAV8(Y733F)-*MYO7A* vectors, the average vestibular hair cell count was 68 ± 4.3 cells/2,500 μm^2 (n = 6 mice, p > 0.9, compared with wild-type mice, ANOVA with Tukey's multiple comparisons test) (Figure 3C). The fact that the vestibular hair cells in shaker-1 mice do not undergo degeneration at this age suggests that the vestibular system in these animals may be more amenable to inner ear gene therapy treatment.

Dual-AAV8(Y733F)-*MYO7A* vectors improve vestibular hair cell stereocilium morphology in shaker-1 mice

Next, we asked whether, in vestibular hair cells, these dual vectors can improve stereocilium bundle organization. Vestibular hair cell stereocilium bundles in wild-type mice are organized in rows of increasing height (Figure 4A), whereas vestibular hair cell stereocilium bundles in shaker-1 mice are highly disorganized (Figure 4A). After injection with dual-AAV8(Y733F)-*MYO7A* vectors, the stereocilium bundles of treated shaker-1 vestibular hair cells became much more organized compared with untreated shaker-1 mice (Figure 4A). The fact that dual-AAV8(Y733F)-*MYO7A* vectors improve stereocilium organization in the vestibular system suggests that the vestibular system is amenable to gene therapy in this mouse model.

Dual-AAV8(Y733F)-*MYO7A* vectors reduce circling behavior in shaker-1 mice

Shaker-1 mice exhibit vestibular dysfunction throughout life. One of the manifestations of vestibular dysfunction in these animals is circling behavior. Wild-type mice typically walk in a straight line, and they like to explore the periphery of their housing cage (Figure 4B). In contrast, shaker-1 mice tend to walk in circles, likely because of significant vestibular dysfunction (Figure 4B). When shaker-1 mice were treated with dual-AAV8(Y733F)-*MYO7A* vectors, we saw a significant reduction in circling behavior (Figure 4B). The circling behavior was quantified by counting the number of circles these animals made in 120 s using a video tracking system (Figure 4C; ANY-Maze video tracking system; Stoelting, Wood Dale, IL, USA). The untreated wild-type and heterozygous littermates made 9.3 ± 1.1 rotations/120 s (n = 10 mice), whereas the untreated shaker-1 mice made 34 ± 4.4 rotations/120 s (n = 4, p = <0.0001 compared with wild-type/heterozygous mice, ANOVA with Tukey's multiple-comparisons test). When shaker-1 mice were treated with dual-AAV8(Y733F)-*MYO7A* vectors, a significant reduction of

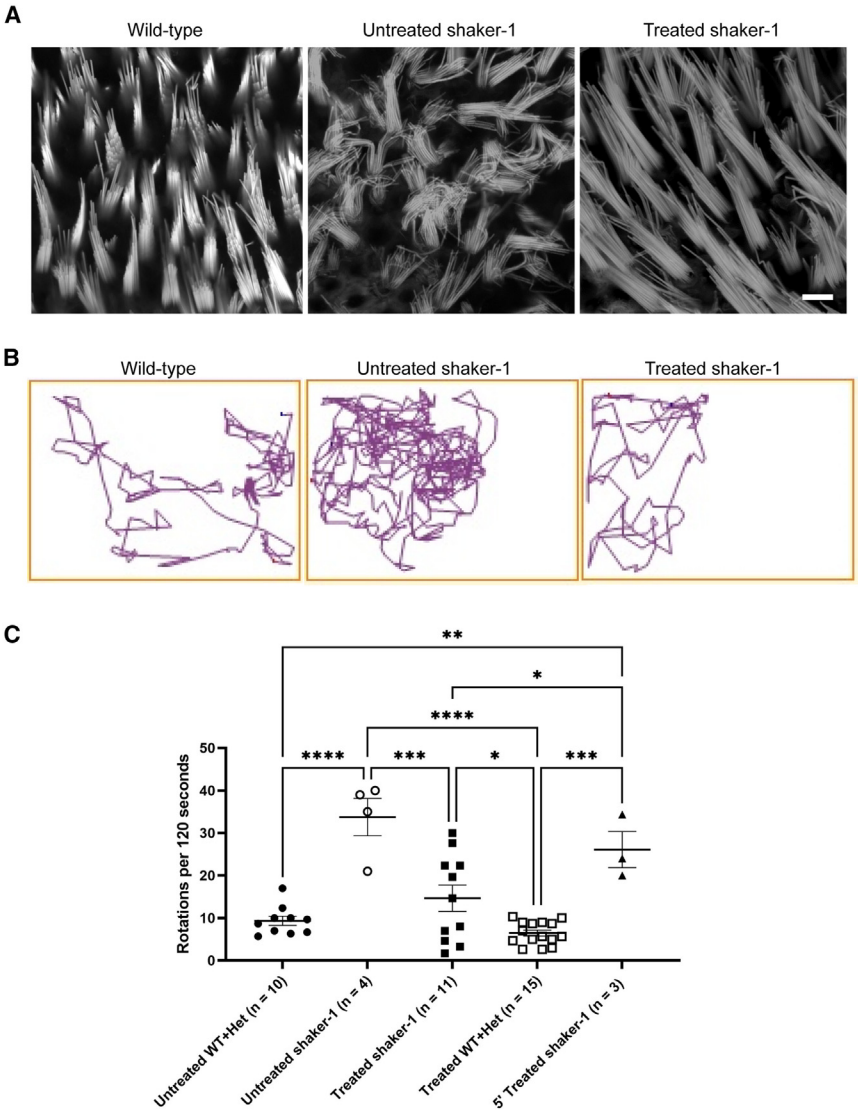

Figure 4. Dual-AAV8(Y733F)-*MYO7A* vectors improve vestibular stereocilium organization and circling behavior in shaker-1 mice

(A) Representative confocal images of stereocilium bundles of vestibular hair cells from mouse utricles stained by phalloidin to visualize F-actin. The shaker-1 vestibular hair cells have highly disorganized stereocilium bundles compared with wild-type hair cells. Shaker-1 mice treated with dual-AAV8(Y733F)-*MYO7A* vectors showed significant improvement in vestibular stereocilium organization compared with untreated shaker-1 vestibular hair cells. The scale bar represents 10 μm. (B) Representative track plots from a wild-type mouse, an untreated shaker-1 mouse, and a shaker-1 mouse treated with dual-AAV8(Y733F)-*MYO7A* vectors. Dual-AAV8(Y733F)-*MYO7A* vectors decreased circling behavior in treated shaker-1 mice. (C) Quantification of circling behavior was performed at ∼P30. Shaker-1 mice that were treated with dual-AAV8(Y733F)-*MYO7A* showed significant reduction in circling compared with untreated shaker-1 mice. Error bars represent standard errors. *$p < 0.05$, **$p < 0.01$, ***$p < 0.001$, ****$p < 0.0001$.

circling behavior was observed. Shaker-1 mice that were injected with dual-AAV8(Y733F)-*MYO7A* vectors made 15 ± 3.1 rotations/120 s, which is significantly reduced compared with untreated shaker-1 mice (n = 11 mice, p = 0.0004 compared with untreated shaker-1 mice, ANOVA with Tukey's multiple-comparisons test). The wild-type and heterozygous littermates that were injected with dual-AAV8(Y733F)-*MYO7A* vectors made 6.5 ± 0.69 rotations/120 s (n = 15 mice). This is similar to untreated wild-type and heterozygous littermates (p = 0.8, ANOVA with Tukey's multiple-comparisons test). No reduction in circling behavior was observed in shaker-1 mice that were treated with 5′ AAV8 (Y733F)-*MYO7A* vector alone (26 ± 4.3 rotations/120 s, n = 3 mice, p = 0.7 compared with untreated shaker-1 mice and $p \leq 0.05$ compared with dual-AAV8(Y733F)-*MYO7A*-treated shaker-1 mice, ANOVA with Tukey's multiple-comparisons test). These data show that dual-AAV8(Y733F)-*MYO7A* vectors are capable of reducing circling behavior in shaker-1 mice, which is an indication of improvement of vestibular function.

Dual-AAV8(Y733F)-*MYO7A* vectors improve vestibular sensory-evoked potential (VsEP) in shaker-1 mice

While circling behavior is often used as a measure for vestibular dysfunction, it is not specific to the vestibular system. To directly assess the impact of dual-AAV8(Y733F)-*MYO7A* gene therapy on the vestibular system in shaker-1 mice, we tested the VsEPs in these animals (Figure 5). VsEPs measure the neural activities of the vestibular system in response to a linear head motion that stimulates the gravity receptor organs (utricle and saccule).[25] In wild-type mice, the average VsEP threshold was −10 ± 1.0 dB (n = 7 mice), whereas in untreated shaker-1 mice, VsEP waveforms were not detected even at the maximal stimulus level of +6 dB, and therefore were designated to have a threshold of +7.5 dB (n = 9 mice, $p < 0.0001$ compared with untreated wild-type/heterozygous littermates, ANOVA with Tukey's multiple-comparisons test). When shaker-1 mice were treated with dual-AAV8(Y733F)-*MYO7A*, VsEP waveforms were detected in many animals (Figure 5A). In shaker-1 mice that were treated with dual-AAV8 (Y733F)-*MYO7A* vectors (n = 13 mice), eight animals had measurable VsEP thresholds, and the average VsEP threshold of all 13 mice was +2.0 ± 1.8 dB (p = 0.04 compared with untreated shaker-1 mice, ANOVA with Tukey's multiple-comparisons test, Figure 5B). The wild-type and heterozygous littermates that were injected with dual-AAV8(Y733F)-*MYO7A* vectors showed similar

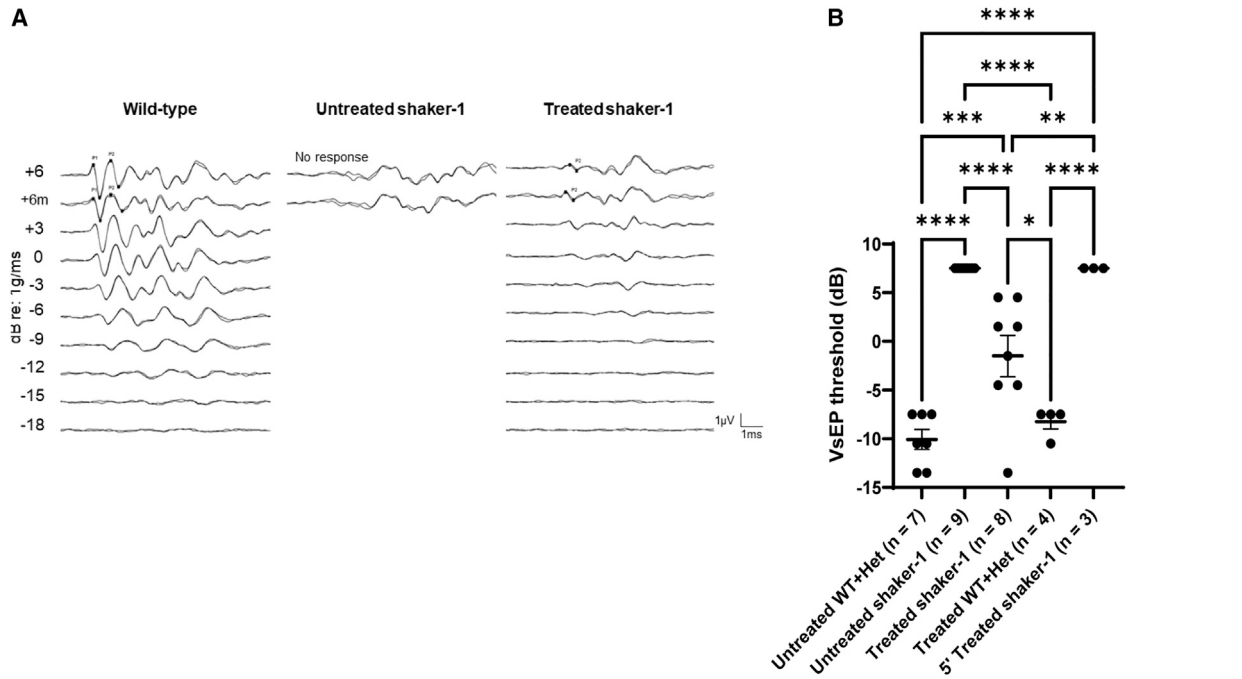

Figure 5. Dual-AAV8(Y733F)-*MYO7A* vectors improved VsEP thresholds in shaker-1 mice

(A) Representative vestibular sensory-evoked potential (VsEP) recordings from a wild-type mouse, an untreated shaker-1 mouse, and a shaker-1 mouse treated with dual-AAV8(Y733F)-*MYO7A* vectors. The untreated shaker-1 mouse had no measurable VsEP responses, whereas the treated shaker-1 mouse had measurable VsEP responses. (B) VsEP threshold measurements. Shaker-1 mice that were treated with dual-AAV8(Y733F)-*MYO7A* vectors showed improvement in VsEP thresholds compared with untreated shaker-1 mice. Error bars represent standard errors. *$p < 0.05$, **$p < 0.01$, ***$p < 0.001$, ****$p < 0.0001$.

VsEP thresholds as untreated wild-type and heterozygous littermates, with the average VsEP threshold being −8.3 ± 0.75 dB (n = 4 mice, $p > 0.9$ compared with untreated wild-type/heterozygous littermates, ANOVA with Tukey's multiple-comparisons test). This suggests that dual-AAV8(Y733F)-*MYO7A* vectors did not cause any toxicity to the vestibular system in shaker-1 mice. The shaker-1 mice that received the 5′ vector alone did not show any measurable VsEP thresholds (+7.5 dB, n = 3 mice), similar to untreated shaker-1 mice. These data indicate that dual-AAV8(Y733F)-*MYO7A* vectors can improve vestibular function in shaker-1 mice.

DISCUSSION

USH is a genetic disease that has a profound impact on a patient's quality of life, particularly those who have type 1 USH, such as USH1B. While patients with USH1B often have profound hearing loss and visual loss, they also experience vestibular dysfunction, which can significantly increase their risk for fall-related injuries. Therefore, our study investigated the effect of gene replacement therapy as a treatment for auditory and vestibular dysfunction in a mouse model of USH1B, the shaker-1 mouse. The shaker-1 mouse (*Myo7a*$^{4626SB/4626SB}$) was generated using N-ethyl-N-nitrosourea (ENU) mutagenesis, which resulted in a premature stop codon (NM_001256081).[17] In mice, the 4626SB mutation in *Myo7a* has been shown to cause abnormal hair cell stereocilium bundle morphology.[26,27] Consequently, shaker-1 mice have profound deafness and vestibular dysfunction. Therefore, the inner ear of the shaker-1 mouse is a good model for USH1B because patients with USH1B also demonstrate profound hearing loss and vestibular dysfunction.

The dual-AAV vector-based approach has been successfully applied in the mouse inner ear. Previously, two studies have shown that the dual-AAV vectors are capable of delivering the otoferlin protein in a DFNB9 mouse model.[12,28] Otoferlin is involved in calcium ion binding activity and synaptic vesicle trafficking.[29,30] Dual-AAV vectors can produce a recombinant full-length otoferlin protein in cells co-infected with 5′ and 3′ vectors, thus restoring otoferlin expression in the inner ear.[12] Similarly, it has been found that injection of dual-AAV-otoferlin vectors partially restores synaptic function in mutant mice.[28] These studies also demonstrated that the dual-AAV vector-based approach improves hearing in a DFNB9 mouse model and corrects profound deafness.[12,28] Furthermore, it has been shown that dual-AAV vectors can prolong hearing recovery over a sustained time period. There was improved auditory function for at least 20 weeks post injection.[12] More recently, the dual-AAV vector-based approach has been shown to successfully improve auditory function in a mouse model of DFNB16.[31] In this case, the dual-AAV vectors employ intein-mediated protein recombination rather than recombination at the DNA level.[31] Taken together, these studies suggest that dual-AAV gene delivery can be successfully applied to mouse models of human hereditary hearing loss to improve their auditory function.

In this study, we applied the dual-AAV vector-based approach to deliver human *MYO7A* cDNA into the shaker-1 mouse inner ear. The dual-AAV vectors we used in this study have been shown to restore MYO7A expression in the mouse retina following sub-retinal injection.[19] We injected the dual-AAV8(Y733F)-*MYO7A* vectors into the inner ear of neonatal shaker-1 mice using the PSC approach. This resulted in successful transduction of IHCs and OHCs in the cochlea. We observed that shaker-1 mice treated with these dual-AAV vectors had improved cochlear hair cell survival, and many of the surviving hair cells expressed MYO7A. This contrasts with the untreated shaker-1 mice that have severe cochlear hair cell degeneration. We also quantified the transduction rates of IHCs and OHCs in the treated animals and found that the transduction rate was higher at the apex than at the base of the cochlea. The lower transduction rate at the cochlear base may in part be due to the fact that cochlear hair cell degeneration is most profound at the cochlear base. Taken together, these results show that dual-AAV8(Y733F)-*MYO7A* vectors have a protective effect on cochlear hair cells and can prolong their survival.

Stereocilium bundles of inner ear hair cells play an important role in hair cell mechanotransduction. Shaker-1 mice have highly disorganized stereocilium bundles, likely because of the absence of MYO7A. While there was significant improvement in cochlear hair cell survival in shaker-1 mice treated with dual-AAV8 (Y733F)-*MYO7A* vectors, we did not see improvements in stereocilium organization in the treated shaker-1 cochlea. The shaker-1 mice treated with dual-AAV8(Y733F)-*MYO7A* vectors had disorganized stereocilium bundles comparable with the stereocilia bundles seen in the untreated shaker-1 mice. These persistent structural deficits in stereocilium bundles correlate with the lack of hearing rescue seen in the treated shaker-1 mice. However, it is important to note that the cochlear hair cells in this mouse model undergo degeneration as early as embryonic day 17.5 (E17.5), and it may be necessary to deliver gene therapy *in utero* to rescue auditory function in these animals.[27] We also observed a 10- to 30-dB ABR threshold elevation in wild-type and heterozygous littermates that were treated with dual-AAV8(Y733F)-*MYO7A* vectors, while wild-type and heterozygous littermates that were treated with virus vehicle did not show significant ABR threshold elevation compared with untreated wild-type and heterozygous animals. In addition, similar ABR threshold elevation was observed in wild-type and heterozygous littermates that were treated with 5′ vector alone or with AAV8(Y733F)-GFP. This suggests that there may be some toxicity associated with the dual-AAV8(Y733F)-*MYO7A* vectors in the cochlea. Interestingly, these were the same hybrid dual-AAV (Y733F) vectors used by Dyka et al.[13] These vectors, used at similar doses as those employed in the current study, led to partial retinal degeneration following subretinal injection. Both results may be attributed to the deleterious effects of truncated protein arising from the 5′ vector or to the AAV8(Y733F) vector itself. Notably, these vectors have since been optimized to prevent production of this truncated protein. Future studies will evaluate their performance in the inner ear.

The vestibular system is integral for maintaining balance and positioning. In contrast to the cochlea, the vestibular hair cells in shaker-1 mice do not undergo degeneration. Their structural maintenance relative to cochlear hair cells likely explains why the vestibular system was more amenable to the beneficial effects of inner ear gene therapy in this mouse model. Shaker-1 mice treated with the dual-AAV8(Y733F)-*MYO7A* vectors show high virus transduction (70%–80%) of vestibular hair cells throughout the utricle. In addition, we observed significant improvement in the organization and cohesion of the vestibular stereocilium bundles in the shaker-1 mice treated with the dual-AAV8(Y733F)-*MYO7A* vectors compared with that seen in the untreated shaker-1 mice.

We examined circling behavior as a measure of vestibular function in shaker-1 mice treated with the dual-AAV8(Y733F)-*MYO7A* vectors. We observed that treated shaker-1 mice had a significant reduction in circling behavior compared with untreated shaker-1 mice. Several shaker-1 mice treated with dual-AAV8(Y733F)-*MYO7A* vectors had a significantly reduced amount of circling behavior comparable with that seen in the wild-type and heterozygous animals. The abnormally high level of circling behavior in shaker-1 mice was not improved with injection of the 5′ vector alone, indicating that the 5′ and 3′ AAV8(Y733F) vectors are necessary for a reduction of circling behavior in shaker-1 mice.

Because circling behavior is an indirect measurement of vestibular function, we assessed VsEPs as a direct test of vestibular function. We found that dual-AAV8(Y733F)-*MYO7A* vectors improved VsEP thresholds in shaker-1 mice. In contrast, the untreated shaker-1 mice did not have measurable VsEP waveforms, even at the highest stimulus level. However, many of the treated shaker-1 mice had measurable VsEP waveforms. In fact, in one treated shaker-1 mouse, the VsEP thresholds were similar to those in the wild type. No VsEP responses were observed in the shaker-1 mice that received 5′ vector alone. In addition, the wild-type and heterozygous littermates that were treated with dual-AAV8(Y733F)-*MYO7A* vectors did not show any increase in circling or elevation of VsEP thresholds, in contrast to the 10- to 30-dB ABR threshold elevation observed in these animals. This suggests that the vestibular system in the shaker-1 mice may be more resistant to the potential toxicity of these dual vectors.

Our study showed that delivery of *MYO7A* cDNA via the dual-AAV8 (Y733F) vectors improved cochlear hair cell survival and vestibular function in shaker-1 mice. In a study by Wafa et al.,[32] a cohort of 90 USH patients who had a molecular genetic diagnosis underwent a battery of vestibular tests to characterize their vestibular dysfunction. They found that all patients with type 1 USH had measurable vestibular abnormality in at least one of the vestibular tests that were performed. In addition, results from sensory organization test showed that many of the type 1 USH patients were at risk for falling,[32] which is the leading cause of injury-related death in US adults older than 65 years of age.[33,34] Furthermore, it has been shown that vestibular hair cells are still present in a human temporal bone specimen

from an elderly patient with USH1B.[35] This demonstrates that the mature vestibular system in USH1B patients may still be viable and amenable to the therapeutic effects of inner ear gene therapy. Our results show that gene replacement therapy with dual-AAV8(Y733F)-*MYO7A* vectors has great translational potential for improving vestibular function in USH1B patients, reducing their risk of falling. It is our hope that the results from this study will serve as a foundation for future clinical translation of gene replacement therapy to help patients with USH1B.

MATERIALS AND METHODS

AAV vector construction

The production of dual-AAV vectors has been described previously.[13] The dual-AAV vectors were produced by the Boye Lab at the University of Florida. They were designed to ultimately deliver the full-length coding sequence of *MYO7A* (human isoform 2; NM_001127180, with an alternatively spliced GTGAAG sequence at the end of exon 46 encoding two additional residues) under control of the ubiquitous smCBA promoter. The 5′ vector contained the smCBA promoter, the 5′ segment of *MYO7A* cDNA (2,904 bp), a highly recombinogenic sequence derived from the AP coding sequence, and a splice donor. The 3′ vector contained a splice acceptor, a complementary AP coding sequence, the 3′ segment (3,627 bp) of *MYO7A* cDNA (with an HA tag), and a polyadenylation signal. Vectors were packaged, purified, and titered as described previously.[36] The viral titer was 6.5×10^{12} GC/mL for the 5′ vector and 1.1×10^{13} GC/mL for the 3′ vector. The AAV8(Y733F)-smCBA-GFP virus was produced in the same facility using a similar protocol. Its viral titer was 7.7×10^{12} GC/mL.

Animals

Mice were housed at the National Institute on Deafness and Other Communication Disorders (NIDCD) animal facility and cared for by NIDCD animal facility staff. The shaker-1 mice used in this study were acquired from Jackson Laboratory and backcrossed with C57BL/6J mice.

AAV infection of COS-7 cells

COS-7 cells were plated on 24 × 24 mm glass coverslips and maintained at 37°C and 5% CO_2 in DMEM supplemented with 5% fetal bovine serum (FBS) until 40%–50% confluence. Cultures were transduced with 2 μL of either 5′ AAV (1.3×10^{10} GC) or 3′ AAV (2.2×10^{10} GC) or a combination of 2 μL of each of 5′ AAV and 3′ AAV diluted in 0.5 mL of culture medium and pre-incubated for 12 h. 1.5 mL of culture medium was added, and cells were incubated for up to 4 days. Cells were then fixed for 20 min in 4% paraformaldehyde in PBS, permeabilized for 10 min in 0.5% Triton X-100 in PBS, and blocked with 5% BSA in PBS for 2 h. Then primary antibodies were applied for 3 h, coverslips were washed 3 times with PBS, secondary antibodies (Thermo Fisher Scientific) were applied for 1 h, and coverslips were washed 3 times with PBS and then mounted on a microscope slide with ProLong Diamond Antifade Mountant (Thermo Fisher Scientific).[37] The primary mouse monoclonal anti-MYO7A antibody directed against amino acids 11–70 was purchased from Santa Cruz Biotechnology (Dallas, TX, USA; catalog number sc-74516, dilution 1/200 in PBS). The immunopurified rabbit anti-MYO7A antibody directed against amino acids 880–1,077 was purchased from Proteus Biosciences (Ramona, CA, USA; catalog number 25-6790, dilution 1/400 in PBS). The immunopurified rabbit anti-HA tag antibody was purchased from Cell Signaling Technology (Danvers, MA, USA; catalog number 3724S, dilution 1/400 in PBS). Cells were counterstained with phalloidin and DAPI. Preparations were scanned in either super-resolution mode or confocal mode using an LSM 880 Airyscan confocal microscope (Carl Zeiss, White Plains, NY, USA).

Animal surgery

All animals used in this study were approved by the animal care and use committee at the NIDCD (protocol number ASP1378). The surgical procedures were performed in accordance with the ethical guidelines of the animal care and use committee at the NIDCD. Hypothermia was used to induce and maintain anesthesia in neonatal mice (P0–P5). Surgery was performed only on the left ear of each animal. To deliver AAV vectors, the PSC approach was used.[23] Briefly, a post-auricular incision was made, and the tissue was dissected to expose the PSC. Care was taken to avoid facial nerve injury during dissection. A Nanoliter Microinjection System (Nanoliter2000; World Precision Instruments, Sarasota, FL, USA) was used to load the dual-AAV vectors into a glass micropipette. The dual-AAV virus was injected over approximately 40 s (3.3×10^9 GC for the 5′ vector and 5.5×10^9 GC for the 3′ vector; total volume, 1 μL). The incision was closed with 5-0 Vicryl sutures and tissue glue (Ethicon, Somerville, NJ, USA).

Auditory and VsEP testing

All mice were tested in the Mouse Auditory Testing Core Facility at the NIDCD. Animals were anesthetized with ketamine (50–75 mg/kg; MWI Animal Health, Boise, ID, USA) and dexdomitor (0.5 mg/kg, MWI Animal Health) via intraperitoneal injections. Puralube ointment was applied to the eyes of mice to prevent corneal damage while the animals remained anesthetized. Stimulus generation and physiological recordings were completed using Tucker-Davis Technologies (Gainesville, FL, USA) hardware (RZ6 Multi I/O Processor) and software (BioSigRx, v.5.1). The electrophysiological activity was amplified 200,000×, filtered (300–3,000 Hz), and digitized (125 kHz).

ABR testing was performed to evaluate hearing sensitivity at ∼P30. Following anesthesia, the animals were placed on a warming pad in a sound booth (ETS-Lindgren Acoustic Systems, Cedar Park, TX, USA). Sub-dermal needle electrodes were inserted at the vertex (+) and test ear mastoid (−) with a ground electrode inserted under the contralateral ear. ABR thresholds were measured at 4, 8, 16, and 32 kHz using 3-ms, Blackman-gated tone pips presented at 29.9/s with alternating stimulus polarity. At each stimulus level, 512–1,024 responses were averaged. Thresholds were determined by visual inspection of the waveforms and defined as the lowest stimulus level at which any wave could be reliably detected. A minimum of two waveforms were obtained at the threshold level to ensure repeatability of the responses. Physiological results were analyzed for

individual frequencies and then averaged for each of these frequencies from 4–32 kHz.

VsEPs were obtained as described previously.[38] Subcutaneous electrodes were placed at the nuchal crest, at the left ear, and at the right hip. Mice were placed in the supine position on the heating pad with the head placed in a custom, non-invasive head clip attached to an electromechanical shaker (ET 132-2; Labworks, Costa Mesa, CA, USA). The shaker delivered linear pulses (2-ms duration, 17 pulses per second) to the head in the naso-occipital axis. An accelerometer attached to the shaker was used to calibrate the stimulus in jerk (i.e., first derivative of acceleration) at the start of each test session. Stimuli were delivered in 3-dB steps from +6 dB to −18 dB re:1.0 g/ms (1.0 g = 9.8 m/s^2). Four waveforms were measured at each stimulus level: two in the positive (occipital toward nasal) and two in the negative (nasal toward occipital) direction (256 responses per waveform). Pairs of the positive and negative waveforms were averaged together to produce two averaged waveforms for analyses. The two averaged waveforms were superimposed and compared to ensure reproducibility. To ensure no contribution of an auditory response to the waveform, testing began with presentation of the highest stimulus level (+6 dB) under quiet conditions and in the presence of a masking noise (50–50,000 Hz, 96-dB SPL). If the unmasked response peak amplitude changed by more than 50% in the presence of the masker, then the test was performed with the masker on. We defined the threshold measured as the stimulus level (dB) halfway between the lowest stimulus level producing a response and the next stimulus level at which no response was measured.

Circling behavior

Circling behavior was characterized and quantified using optical tracking and the ANY-Maze tracking software (Stoelting). The mice were placed in a 38 × 58 cm box with a video camera (Fujinon YV5X2.7R4B-2 1/3-inch 2.7–13.5 mm F1.3 Day/Night Aspherical Vari-Focal Lens, Fujifilm) directly above. The ANY-Maze software was set to track the movements of the mice placed in the box. We placed each mouse into the box and allowed 2 min for the mouse to become acclimatized to the new environment. The number of rotations, speed, and distance traveled were recorded over a 2-min period for each trial with a 1-min "cool-down" period between trials where no data was recorded. Three trials were performed for each mouse, and the average was calculated. Testing was performed at approximately P30.

Immunohistochemistry

After auditory testing, the mice were euthanized by CO_2 asphyxiation followed by decapitation. Temporal bones were harvested and fixed overnight with formaldehyde (4% paraformaldehyde solution in 1× PBS) followed by decalcification in 120 mM disodium EDTA for 4 days. The vestibular organs and cochlear sensory epithelia were micro-dissected, blocked with normal goat serum in PBS, and labeled with the mouse anti-MYO7A antibody to label hair cells (1:200, product 25-6790, Proteus Biosciences), and with chicken anti-GFP antibody (1:1,000, product ab13970; Abcam, Cambridge, MA, USA). Primary and secondary antibodies were diluted in PBS.

Quantification and transduction efficiency measurements

Z stacks of images were obtained using a Carl Zeiss LSM880 confocal microscope using 10× and 63× objectives. Images were taken for quantification of hair cells and calculation of the viral transduction efficiency. Two images were taken with a 63×, 1.4 N.A. objective at the three turns of the cochlea: apex, middle, and base. To ensure consistency between quantification of images, the pictures were taken at opposite ends of each cochlear turn. The total IHCs and OHCs were counted in a 136-μm segment of each turn and reported on an Excel sheet. Because shaker-1 mice do not express MYO7A, the total number of surviving hair cells was calculated by counting the hair cells with stereocilium bundles, labeled by phalloidin. The transduction efficiency was calculated by dividing the number of hair cells expressing MYO7A, indicating virus transduction, by the total number of hair cells in a 136-μm segment. The total number of hair cells and infection rates were calculated separately for IHCs and OHCs.

For each animal, two images were taken from the utricle in the extrastriolar region using a 63×, 1.4 N.A. objective. The imaging location was consistent across all specimens. To quantify the number of vestibular hair cells, a 50 × 50 μm box was placed within each z-stacked image. The location of these boxes was consistent across all specimens. All hair cells in the box were counted and quantified. The total number of surviving hair cells was calculated by counting the hair cells with stereocilium bundles, labeled by phalloidin. To measure the transduction efficiency of vestibular hair cells, we divided the number of infected cells that expressed MYO7A by the total number of hair cells in a 50 × 50 μm area of interest. After calculating the total number of utricular hair cells and infection rate for the two images, the quantification and transduction rates were averaged.

Statistics

ANOVA and Tukey's multiple-comparisons test were used to determine the statistical significance when comparing measurements for hair cell quantification and transduction rates. ANOVA and Tukey's multiple-comparisons test were also used to analyze the statistical significance in ABR thresholds, circling behavior, and VsEP thresholds. A p value of less than 0.05 indicates statistical significance.

DATA AND CODE AVAILABILITY

Data will be made available upon request.

SUPPLEMENTAL INFORMATION

Supplemental information can be found online at https://doi.org/10.1016/j.omtm.2023.08.012.

ACKNOWLEDGMENTS

This work is supported by NIDCD Division of Intramural Research grants DC000082-02 (to W.W.C.), DC000039 (to T.B.F.), DC000080 (to the Mouse Auditory Testing Core), and National Eye Institute grant R01EY024280 (to S.E.B.). This research was

made possible through the NIH Medical Research Scholars Program, a public-private partnership supported jointly by the NIH and contributions to the NIH from the Doris Duke Charitable Foundation (DDCF grant 2014194), the American Association for Dental Research, the Colgate-Palmolive Company, Genentech, Elsevier, and other private donors. We are also grateful for the NIDCD animal facility staff for caring for our animals.

AUTHOR CONTRIBUTIONS

W.W.C., S.E.B., S.L.B., I.A.B., and T.B.F. conceived and designed the study. S.C.L., M.G., K.I., M.S., K.R.C., J.L.Z., Y.I., Z.O., T.W., T.F., and W.W.C. performed the experiment and analyzed the data. W.W.C. and M.G. supervised the work. S.C.L., M.G., and W.W.C. wrote the manuscript with participation of all authors.

DECLARATION OF INTERESTS

S.E.B. and S.L.B. are founders and consultants for Atsena Therapeutics.

REFERENCES

1. Vernon, M. (1969). Usher's syndrome–deafness and progressive blindness. Clinical cases, prevention, theory and literature survey. J. Chron. Dis. *22*, 133–151. https://doi.org/10.1016/0021-9681(69)90055-1.

2. Saihan, Z., Webster, A.R., Luxon, L., and Bitner-Glindzicz, M. (2009). Update on Usher syndrome. Curr. Opin. Neurol. *22*, 19–27.

3. Galbis-Martínez, L., Blanco-Kelly, F., García-García, G., Ávila-Fernández, A., Jaijo, T., Fuster-García, C., Perea-Romero, I., Zurita-Muñoz, O., Jimenez-Rolando, B., Carreño, E., et al. (2021). Genotype-phenotype correlation in patients with Usher syndrome and pathogenic variants in MYO7A: implications for future clinical trials. Acta Ophthalmol. *99*, 922–930. https://doi.org/10.1111/aos.14795.

4. Toms, M., Pagarkar, W., and Moosajee, M. (2020). Usher syndrome: clinical features, molecular genetics and advancing therapeutics. Ther. Adv. Ophthalmol. *12*. 2515841420952194. https://doi.org/10.1177/2515841420952194.

5. Jouret, G., Poirsier, C., Spodenkiewicz, M., Jaquin, C., Gouy, E., Arndt, C., Labrousse, M., Gaillard, D., Doco-Fenzy, M., and Lebre, A.S. (2019). Genetics of Usher Syndrome: New Insights From a Meta-analysis. Otol. Neurotol. *40*, 121–129. https://doi.org/10.1097/MAO.0000000000002054.

6. Petit, C. (2001). Usher syndrome: from genetics to pathogenesis. Annu. Rev. Genom. Hum. Genet. *2*, 271–297.

7. Ouyang, X.M., Yan, D., Du, L.L., Hejtmancik, J.F., Jacobson, S.G., Nance, W.E., Li, A.R., Angeli, S., Kaiser, M., Newton, V., et al. (2005). Characterization of Usher syndrome type I gene mutations in an Usher syndrome patient population. Hum. Genet. *116*, 292–299. https://doi.org/10.1007/s00439-004-1227-2.

8. Castiglione, A., and Möller, C. (2022). Usher Syndrome. Audiol. Res. *12*, 42–65. https://doi.org/10.3390/audiolres12010005.

9. Lu, Y., Zhou, D., King, R., Zhu, S., Simpson, C.L., Jones, B.C., Zhang, W., Geisert, E.E., and Lu, L. (2018). The genetic dissection of Myo7a gene expression in the retinas of BXD mice. Mol. Vis. *24*, 115–126.

10. Géléoc, G.G.S., and El-Amraoui, A. (2020). Disease mechanisms and gene therapy for Usher syndrome. Hear. Res. *394*, 107932. https://doi.org/10.1016/j.heares.2020.107932.

11. Lopes, V.S., Boye, S.E., Louie, C.M., Boye, S., Dyka, F., Chiodo, V., Fofo, H., Hauswirth, W.W., and Williams, D.S. (2013). Retinal gene therapy with a large MYO7A cDNA using adeno-associated virus. Gene Ther. *20*, 824–833. https://doi.org/10.1038/gt.2013.3.

12. Akil, O., Dyka, F., Calvet, C., Emptoz, A., Lahlou, G., Nouaille, S., Boutet de Monvel, J., Hardelin, J.P., Hauswirth, W.W., Avan, P., et al. (2019). Dual AAV-mediated gene therapy restores hearing in a DFNB9 mouse model. Proc. Natl. Acad. Sci. USA *116*, 4496–4501. https://doi.org/10.1073/pnas.1817537116.

13. Dyka, F.M., Boye, S.L., Chiodo, V.A., Hauswirth, W.W., and Boye, S.E. (2014). Dual adeno-associated virus vectors result in efficient in vitro and in vivo expression of an oversized gene, MYO7A. Hum. Gene Ther. Methods *25*, 166–177. https://doi.org/10.1089/hgtb.2013.212.

14. Trapani, I., Colella, P., Sommella, A., Iodice, C., Cesi, G., de Simone, S., Marrocco, E., Rossi, S., Giunti, M., Palfi, A., et al. (2014). Effective delivery of large genes to the retina by dual AAV vectors. EMBO Mol. Med. *6*, 194–211. https://doi.org/10.1002/emmm.201302948.

15. Ghosh, A., Yue, Y., and Duan, D. (2011). Efficient transgene reconstitution with hybrid dual AAV vectors carrying the minimized bridging sequences. Hum. Gene Ther. *22*, 77–83. https://doi.org/10.1089/hum.2010.122.

16. Gibson, F., Walsh, J., Mburu, P., Varela, A., Brown, K.A., Antonio, M., Beisel, K.W., Steel, K.P., and Brown, S.D. (1995). A type VII myosin encoded by the mouse deafness gene shaker-1. Nature *374*, 62–64. https://doi.org/10.1038/374062a0.

17. Hasson, T., Walsh, J., Cable, J., Mooseker, M.S., Brown, S.D., and Steel, K.P. (1997). Effects of shaker-1 mutations on myosin-VIIa protein and mRNA expression. Cell Motil Cytoskeleton *37*, 127–138. https://doi.org/10.1002/(SICI)1097-0169(1997)37:2<127::AID-CM5>3.0.CO;2-5.

18. Mburu, P., Liu, X.Z., Walsh, J., Saw, D., Jr., Cope, M.J., Gibson, F., Kendrick-Jones, J., Steel, K.P., and Brown, S.D. (1997). Mutation analysis of the mouse myosin VIIA deafness gene. Gene Funct. *1*, 191–203. https://doi.org/10.1046/j.1365-4624.1997.00020.x.

19. Calabro, K.R., Boye, S., Choudhury, S., McCullough, K.T., Fajardo, D., Strang, C.E., Chakraborty, D., Witherspoon, C.D., Gamlin, P., and Boye, S. (2019). Investigating Dual AAV-Based Treatments for MYO7A Usher Syndrome in Myo7a-/- Mice and Macaque. Mol. Ther. *27*, 316–317.

20. Morgan, C.P., Krey, J.F., Grati, M., Zhao, B., Fallen, S., Kannan-Sundhari, A., Liu, X.Z., Choi, D., Müller, U., and Barr-Gillespie, P.G. (2016). PDZD7-MYO7A complex identified in enriched stereocilia membranes. Elife *5*, e18312. https://doi.org/10.7554/eLife.18312.

21. Grati, M., Shin, J.B., Weston, M.D., Green, J., Bhat, M.A., Gillespie, P.G., and Kachar, B. (2012). Localization of PDZD7 to the stereocilia ankle-link associates this scaffolding protein with the Usher syndrome protein network. J. Neurosci. *32*, 14288–14293. https://doi.org/10.1523/JNEUROSCI.3071-12.2012.

22. Shnerson, A., Lenoir, M., van de Water, T.R., and Pujol, R. (1983). The pattern of sensorineural degeneration in the cochlea of the deaf shaker-1 mouse: ultrastructural observations. Brain Res. *285*, 305–315. https://doi.org/10.1016/0165-3806(83)90028-7.

23. Isgrig, K., and Chien, W.W. (2018). Posterior Semicircular Canal Approach for Inner Ear Gene Delivery in Neonatal Mouse. J. Vis. Exp. https://doi.org/10.103791/56648.

24. Isgrig, K., Shteamer, J.W., Belyantseva, I.A., Drummond, M.C., Fitzgerald, T.S., Vijayakumar, S., Jones, S.M., Griffith, A.J., Friedman, T.B., Cunningham, L.L., and Chien, W.W. (2017). Gene Therapy Restores Balance and Auditory Functions in a Mouse Model of Usher Syndrome. Mol. Ther. *25*, 780–791. https://doi.org/10.1016/j.ymthe.2017.01.007.

25. Jones, S.M., Subramanian, G., Avniel, W., Guo, Y., Burkard, R.F., and Jones, T.A. (2002). Stimulus and recording variables and their effects on mammalian vestibular evoked potentials. J. Neurosci. Methods *118*, 23–31.

26. Prosser, H.M., Rzadzinska, A.K., Steel, K.P., and Bradley, A. (2008). Mosaic complementation demonstrates a regulatory role for myosin VIIa in actin dynamics of stereocilia. Mol. Cell Biol. *28*, 1702–1712. https://doi.org/10.1128/mcb.01282-07.

27. Lefèvre, G., Michel, V., Weil, D., Lepelletier, L., Bizard, E., Wolfrum, U., Hardelin, J.P., and Petit, C. (2008). A core cochlear phenotype in USH1 mouse mutants implicates fibrous links of the hair bundle in its cohesion, orientation and differential growth. Development *135*, 1427–1437. https://doi.org/10.1242/dev.012922.

28. Al-Moyed, H., Cepeda, A.P., Jung, S., Moser, T., Kügler, S., and Reisinger, E. (2019). A dual-AAV approach restores fast exocytosis and partially rescues auditory function in deaf otoferlin knock-out mice. EMBO Mol. Med. *11*, e9396. https://doi.org/10.15252/emmm.201809396.

29. Roux, I., Safieddine, S., Nouvian, R., Grati, M., Simmler, M.-C., Bahloul, A., Perfettini, I., Le Gall, M., Rostaing, P., Hamard, G., et al. (2006). Otoferlin, Defective in a Human Deafness Form, Is Essential for Exocytosis at the Auditory Ribbon Synapse. Cell *127*, 277–289. https://doi.org/10.1016/j.cell.2006.08.040.

30. Yasunaga, S., Grati, M., Cohen-Salmon, M., El-Amraoui, A., Mustapha, M., Salem, N., El-Zir, E., Loiselet, J., and Petit, C. (1999). A mutation in OTOF, encoding otoferlin, a FER-1-like protein, causes DFNB9, a nonsyndromic form of deafness. Nat. Genet. *21*, 363–369. https://doi.org/10.1038/7693.

31. Shubina-Oleinik, O., Nist-Lund, C., French, C., Rockowitz, S., Shearer, A.E., and Holt, J.R. (2021). Dual-vector gene therapy restores cochlear amplification and auditory sensitivity in a mouse model of DFNB16 hearing loss. Sci. Adv. *7*, eabi7629. https://doi.org/10.1126/sciadv.abi7629.

32. Wafa, T.T., Faridi, R., King, K.A., Zalewski, C., Yousaf, R., Schultz, J.M., Morell, R.J., Muskett, J., Turriff, A., Tsilou, E., et al. (2021). Vestibular phenotype-genotype correlation in a cohort of 90 patients with Usher syndrome. Clin. Genet. *99*, 226–235. https://doi.org/10.1111/cge.13868.

33. Stevens, J.A., Corso, P.S., Finkelstein, E.A., and Miller, T.R. (2006). The costs of fatal and non-fatal falls among older adults. Inj. Prev. *12*, 290–295. https://doi.org/10.1136/ip.2005.011015.

34. Gelbard, R., Inaba, K., Okoye, O.T., Morrell, M., Saadi, Z., Lam, L., Talving, P., and Demetriades, D. (2014). Falls in the elderly: a modern look at an old problem. Am. J. Surg. *208*, 249–253. https://doi.org/10.1016/j.amjsurg.2013.12.034.

35. Osgood, R.T., Zhu, M.Y., Jennifer, T., O'Malley, Chien, W., Cremers, C., Nadol, J.B., Jr., Charles Liberman, M., Quesnel, A.M., and Indzhykulian, A.A. (2022). Vestibular Hair Cell Survival and Stereocilia Bundle Morphology in Usher Syndrome Type 1 Patients. The Association for Research in Otolaryngology (ARO) - the 45th Annual MidWinter Meeting.

36. Zolotukhin, S., Potter, M., Zolotukhin, I., Sakai, Y., Loiler, S., Fraites, T.J., Jr., Chiodo, V.A., Phillipsberg, T., Muzyczka, N., Hauswirth, W.W., et al. (2002). Production and purification of serotype 1, 2, and 5 recombinant adeno-associated viral vectors. Methods *28*, 158–167. https://doi.org/10.1016/s1046-2023(02)00220-7.

37. Grati, M., and Kachar, B. (2011). Myosin VIIa and sans localization at stereocilia upper tip-link density implicates these Usher syndrome proteins in mechanotransduction. Proc. Natl. Acad. Sci. USA *108*, 11476–11481. https://doi.org/10.1073/pnas.1104161108.

38. Tona, R., Chen, W., Nakano, Y., Reyes, L.D., Petralia, R.S., Wang, Y.-X., Starost, M.F., Wafa, T.T., Morell, R.J., Cravedi, K.D., et al. (2019). The phenotypic landscape of a Tbc1d24 mutant mouse includes convulsive seizures resembling human early infantile epileptic encephalopathy. Hum. Mol. Genet. *28*, 1530–1547. https://doi.org/10.1093/hmg/ddy445.

OMTM, Volume *30*

Supplemental information

Dual-AAV vector-mediated expression of *MYO7A* improves vestibular function in a mouse model of Usher syndrome 1B

Samantha C. Lau, Mhamed Grati, Kevin Isgrig, Moaz Sinan, Kaitlyn R. Calabro, Jianliang Zhu, Yasuko Ishibashi, Zeynep Ozgur, Talah Wafa, Inna A. Belyantseva, Tracy Fitzgerald, Thomas B. Friedman, Sanford L. Boye, Shannon E. Boye, and Wade W. Chien

Supplemental Figures

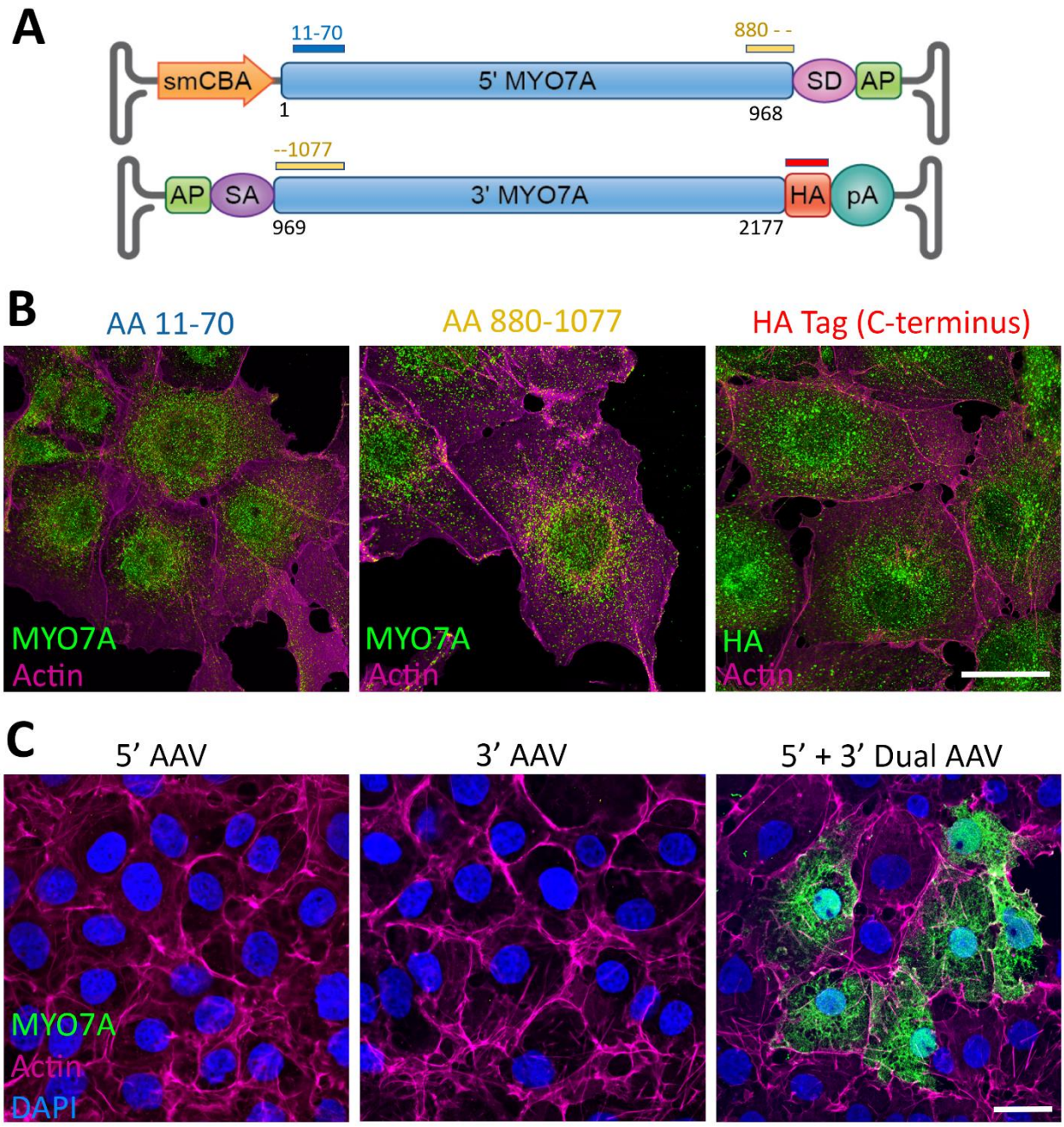

Figure S1. Dual-AAV8(Y733F)-*MYO7A* vectors expressed full-length MYO7A in COS-7 cells. (A) Schematics of the dual-AAV8(Y733F)-MYO7A vectors used in this study. The

human *MYO7A* cDNA was separated into two halves (labeled “5’ *MYO7A*” and “3’ *MYO7A*”), and its expression was driven by the CMV/chicken β-actin promoter (labeled “smCBA”), which was only present in the 5’ vector. The 3’ vector had a polyadenylation signal (pA). The highly recombinogenic coding sequence for alkaline phosphatase (AP), splice donor sites (SD), and splice acceptor sites (SA) were used to facilitate the recombination of the 5’ and 3’ cDNAs. The location of the antigens targeted by both anti-MYO7A antibodies as well as the C-terminal HA tag are marked with color coded rectangles. (B) COS-7 cells were infected with the dual-AAV8(Y733F)-MYO7A vectors which resulted in the expression of full-length human MYO7A. Specimens were imaged using super-resolution AiryScan mode. MYO7A was detected using the anti-MYO7A antibodies directed against the N-terminus, middle, and C-terminus (anti-HA), with very similar cellular distribution across the three specimens. HA refers to the hemagglutinin tag inserted at the C-terminus which facilitates its detection. Scale bar represents 20 μm. (C) COS-7 cells infected with either the 5’ or 3’ vector alone showed no MYO7A expression when the anti-MYO7A antibody targeting the middle portion of the protein was used (AA880-1077). Specimens were imaged using confocal mode. MYO7A expression was detected when both the 5’ and 3’ vectors were simultaneously used. Scale bar represents 20 μm.

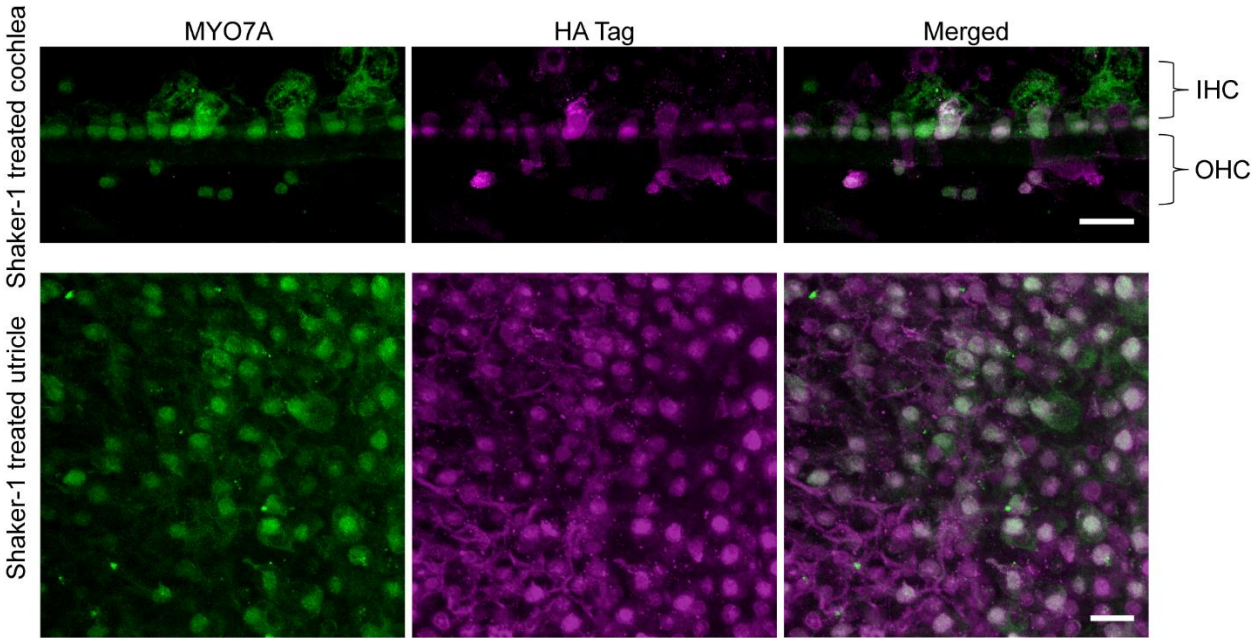

Figure S2. MYO7A co-localized with anti-HA antibodies in treated shaker-1 cochlear and vestibular hair cells. Representative confocal images of the cochlea (top row) and the utricle (bottom row) from a shaker-1 mouse treated with dual-AAV8(Y733F)-*MYO7A* vectors. MYO7A expression in the cochlear and vestibular hair cells of the treated shaker-1 mice co-localized with HA expression. This demonstrates that MYO7A expression in treated shaker-1 mice is mediated by the dual-AAV vectors. The top scale bar from the cochlea represents 20 µm. The bottom scale bar from the utricle represents 10 µm.

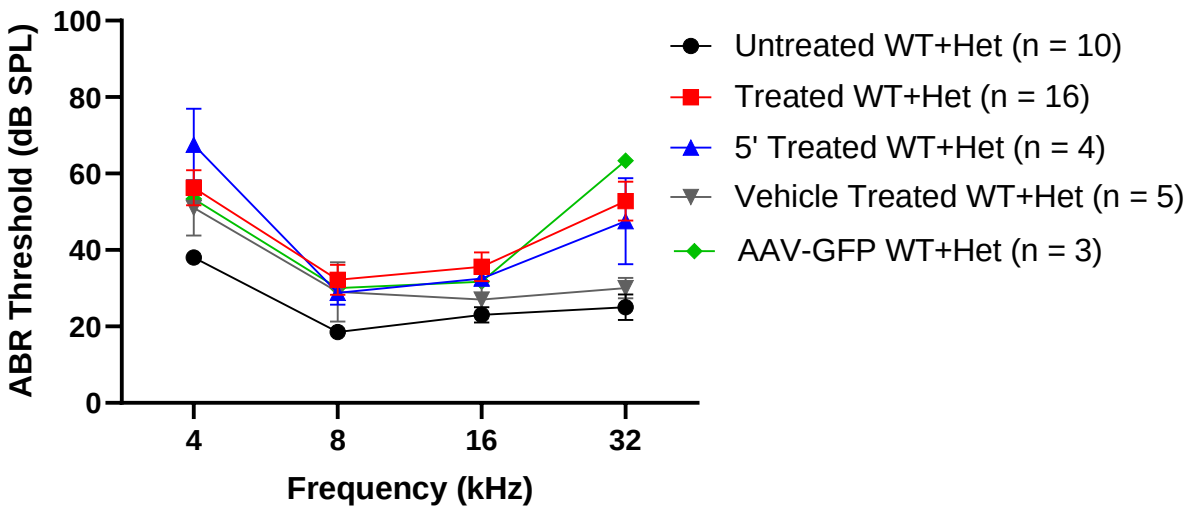

Figure S3. Dual-AAV8(Y733F)-*MYO7A* vectors cause an ABR threshold elevation in wild-type and heterozygous littermates. Auditory brainstem response (ABR) thresholds at the four measured frequencies (4, 8, 16, 32 kHz) are shown. ABR testing was done at ~P30. Injection of dual-AAV8(Y733F)-*MYO7A* vectors (labeled “Treated WT+Het”), 5’ vector alone (labeled “5’ Treated WT+Het”), and AAV8(Y733F)-GFP (labeled “AAV-GFP WT+Het”) caused a 10-30 dB ABR threshold elevation in the wild-type (WT) and heterozygous littermates. In contrast, wild-type and heterozygous littermates that were injected with vehicle (PBS with 5% glycerol, labeled “Vehicle Treated WT+Het”) did not show significant ABR threshold elevation compared to untreated wild-type and heterozygous mice (labeled “Untreated WT+Het”). Error bars represent standard errors.